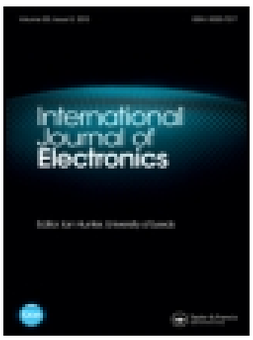

International Journal of Electronics

ISSN: 0020-7217 (Print) 1362-3060 (Online) Journal homepage: https://www.tandfonline.com/loi/tetn20

Electronic band-gap integrated low mutual coupling dual-band MIMO antenna

T. Maturi & Baranikunta Harikrishna

To cite this article: T. Maturi & Baranikunta Harikrishna (2020): Electronic band-gap integrated low mutual coupling dual-band MIMO antenna, International Journal of Electronics

To link to this article: https://doi.org/10.1080/00207217.2020.1726483

Published online: 09 Mar 2020.

INTERNATIONAL JOURNAL OF ELECTRONICS
https://doi.org/10.1080/00207217.2020.1726483

Taylor & Francis
Taylor & Francis Group

Electronic band-gap integrated low mutual coupling dual-band MIMO antenna

T. Maturi[a] and Baranikunta Harikrishna[b]

[a]Electronics and Communication Engineering Department, Shri Jagdishprasad Jhabarmal Tibrewala University, Vidyanagari, India; [b]Electronics and Communication Engineering Department, CMR Engineering College, Hyderabad, India

ABSTRACT

In this paper, a reduced mutual coupling dual-band multiple-input-multiple-output (MIMO) antenna is reported. A thin rectangular slot is incorporated into an unlicensed 5.2 GHz band rectangular patch antenna (RPA) to excite another industrial, scientific and medical (ISM) 2.4 GHz band. In the 1×2 MIMO configuration, antennas are closely placed at a distance of $\lambda_{max}/8$ and the mutual coupling between antenna elements is suppressed by incorporating a dual-band electronics-bandgap (EBG) structure. A mushroom kind of EBG arrangement with two different square-shaped plates on the top and the bottom of the EBG is done to exhibit dual-band rejection characteristics. MIMO communication parameters, envelope correlation coefficient (ECC), diversity gain (DG), and multiplexing efficiency (η_{MUX}) are calculated exhibiting excellent performance of the proposed antenna. Prototype of the antenna is fabricated and good agreement is found amongst simulation and measured results.

ARTICLE HISTORY
Received 9 December 2018
Accepted 30 November 2019

KEYWORDS
Diversity gain; electronic bandgap; envelope correlation coefficient; MIMO antenna; multiplexing efficiency; rectangular patch antenna

1. Introduction

The MIMO antennas have a tradeoff between its size and mutual coupling (Caimi, 2011). When two antennas are placed closer to each other (within near-field regions) they experience strong mutual coupling, resulting in higher envelope correlation coefficient, poor diversity gain, and lower multiplexing efficiency. If antennas are placed far apart ($\approx \lambda/2$ separation), the overall size of the MIMO antenna increases.

Different techniques have been reported in the literature to optimise the tradeoff between MIMO antenna size and its performance. In (Zhu & Eleftheriades, 2010), a field cancellation technique is reported using surface modification to minimise the mutual coupling. However, the effect of the surface modification on other antenna parameters as radiation pattern, gain, and radiation efficiency is not discussed. Iqbal et al. have reported an F-shaped stub integrated partial ground plane structure to reduce the mutual coupling between closely placed ultra-wideband (UWB) antennas (Iqbal, Saraereh, Ahmad, & Bashir, 2017). The reported antenna is resonating in UWB range but the mutual coupling is suppressed only for a narrowband of the operating band. An eight ports dual-band MIMO

CONTACT T. Maturi tirupatikrishna15@gmail.com Electronics and Communication Engineering Department, Shri Jagdishprasad Jhabarmal Tibrewala University, Vidyanagari, Rajasthan 333001, India

antenna array is reported in (Xia, Chen, & Tang, 2015) has suppressed the mutual coupling through orthogonal dual-feeding. The dual-band resonance is introduced by incorporating two symmetrical rectangular slots into the patch, forming E-shaped structure. The antenna elements are separated at a larger distance ($\approx \lambda_{max}/5$) which is increasing the overall size and helping to achieve an isolation better that −20 dB in both operating bands. Where $\approx \lambda_{max}$ is the wavelength of the lowest operating band. A parallel-coupled line is used in Vishvaksenan, Mithra, Kalaiarasan, & Raj (2017) to minimise the mutual coupling between closely placed rectangular patch antennas operating in a single narrowband. In Park, Son, & Raj (2017), an H-shaped conducting wall is placed between single-narrowband rectangular patch antenna to achieve an excellent isolation better than −20 dB.

Since decades, different electronic bandgap structures (EBGs) are being used to suppress the mutual coupling between antennas. Yang et al. have placed a traditional mushroom type EBG structure between two conventional rectangular patch antenna to suppress the mutual coupling (Yang & Samii, 2003). In (Jiao, Jiang, & Li, 2017), multilayered stacked EBG structure is used to reduce the mutual coupling. However, those EBG structures are limited to a single narrowband operation. Kumar has also reported a 1 × 2 wideband MIMO antenna and placed a traditional EBG structure to achieve an isolation of better than −12 dB in entire operating band (Kumar, 2016; Kumar & Shirgan, 2014). In (Mohamadzade & Afsahi, 2017), a single-band planar EBG is presented to achieve an isolation of −33.06 dB between two conventional rectangular patch antenna. The antennas are placed far apart ($\approx \lambda_{max}/3.33$) resulting in better isolation but larger size. Different EBG structures, meander line-based (Hwangbo, Yang, & Yoon, 2017), serpentine (Arun et al., 2017), chequerboard (Gholipour, Azadi-Tinat, & Ghalibafan, 2019), and uniplanar (Dabas, Gangwar, Kanaujia, & Gautam, 2018) type EBG structures are utilised to suppress the mutual coupling for the narrowband or the wideband applications. Similarly, metamaterial-based electronic bandgap structures are placed between elements of the single-band MIMO antenna to suppress the isolation (Yu, Li, & Liu, 2018). However, metamaterials are also used for the gain enhancement (Luo, Li, Xia, & Zhang, 2018) and there are some dedicated developments (Zhao et al., 2017) for the coupling cancellation. In some recent investigations, modified mushroom type EBG is found effective for the multiband operations (Bhavarthe, Rathod, & Reddy, 2019; Jaglan et al., 2018). Jaglan et al. have used the traditional mushroom type EBG unit cells of different dimensions to achieve the multi-band notch characteristics (Jaglan et al., 2018). In (Bhavarthe et al., 2019), the upper layer of the mushroom type EBG is slotted and multiple vias are placed to introduce the dual-band rejection characteristics.

The growing demand for high data transmission rate creates the need for multichannel/multiband communication systems with higher channel capacity. The multiband MIMO communication system is an evolving technology which can meet the current and future requirements (Li et al., 2018; Luo et al., 2019). However, most of the mutual coupling techniques reported in the literature are either dealing with single-narrowband or wideband designs. Thus, it creates a need for novel developments for mutual coupling reduction between antenna elements of the multiband MIMO antennas.

In this work, a dual-band rectangular patch antenna is designed for ISM 2.4 GHz and unlicensed 5.2 GHz. The dual-band antenna is used as a single element of a 1 × 2 MIMO configuration. Two antenna elements are closely placed ($\lambda_{max}/8$) distance and an isolation

of better than −25 dB is achieved. Where λ_{max} is the wavelength of a lower operating band (ISM 2.4 GHz). Since the near-field region of the lower band is larger, a modified mushroom-shaped RBG is integrated to suppress the mutual coupling for both bands. The antenna elements are placed on a common substrate in such a way that it slightly cancels the fields at ISM 2.4 GHz bands from each other leading to lower mutual coupling at lower band than upper band unlike a traditional MIMO antenna.

Later, a dual-band-modified mushroom type EBG is placed between two antenna elements resulting in excellent isolation in both operating bands. The MIMO communication parameters, ECC, DG, and η_{MUX} are calculated and found satisfactory. The prototype of the antenna is developed and considerable agreement is found between simulation and measurement results. The excellent, isolation, good MIMO communication parameters, and operation in popular ISM bands make this antenna useful for many wireless communication systems.

2. Dual-band antenna

In this section, a dual-band single element microstrip antenna is designed which is further used to realise a 1 × 2 MIMO antenna. The layout of the 1 × 2 MIMO antenna is shown in Figure 1. The proposed antenna is built on a commonly used FR4 substrate of thickness 1.6 mm and dielectric constant of 4.4. Initially, a conventional unlicensed 5.2 GHz band rectangular patch antenna is designed. Dimensions, width (W), and length (L) of the conventional rectangular patch antenna are calculated using traditional expressions (1–2) (Balanis, 2012) and later optimised to while introducing dual-band characteristics.

$$W = \frac{c}{2f_r}\sqrt{\frac{2}{\varepsilon_r + 1}} \tag{1}$$

$$L = \frac{1}{2f_r\sqrt{\varepsilon_{reff}}\sqrt{\mu_0\varepsilon_0}} - 2\Delta L \tag{2}$$

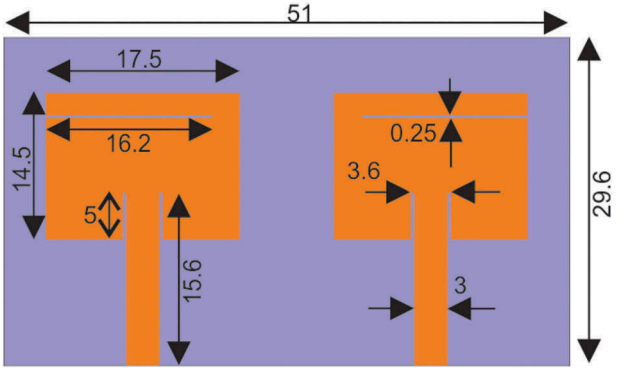

Figure 1. Layout of the top view of the dual-band antenna. Width and length of the ground plane are equal to the substrate dimensions (units mm).

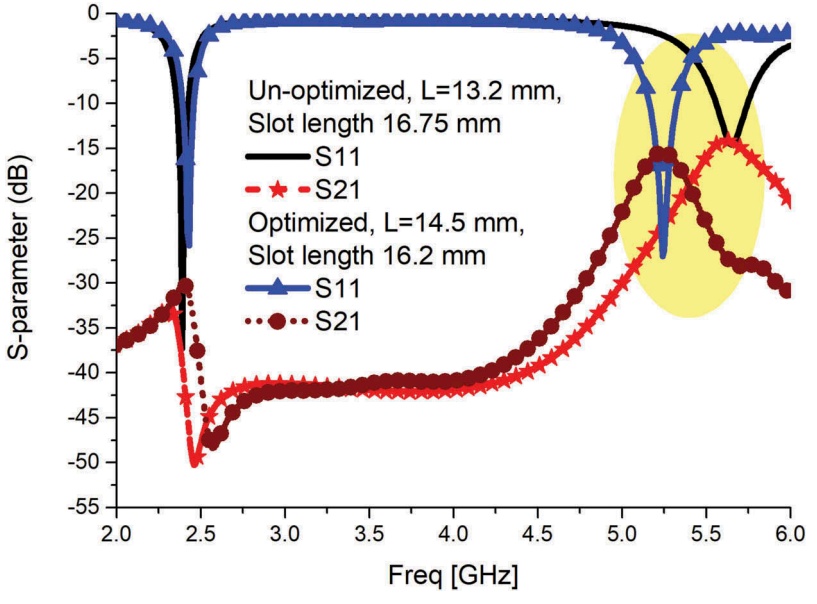

Figure 2. Scattering parameter of dual-band MIMO antenna.

where c is speed of light, f_r is resonant frequency, ε_0 is permittivity, ε_r is relative permittivity, ε_{reff} is effective relative permittivity, μ_0 is relative permeability, and ΔL is the increase in length due to the fringing effect. Thereafter, an optimised thin rectangular slot is placed along the length of the patch to excite another 2.4 GHz ISM band. The scattering parameters, surface current distributions, and 3D-polar plot of the antenna total gain are presented in Figures 2 and 3 respectively. By incorporating rectangular slots into patches dual-band operation is achieved. However, incorporating a slot into the patch shift the actual operating frequency of conventional 5.2 GHz band, as shown in Figure 2. Thus, the length (L) of the patch and length of the slot is precisely optimised to achieve exact ISM 2.4 GHz and unlicensed 5.2 GHz. It is evident in Figure 2 that the optimised length of the patch and length of the slot meet the exact desired ISM 2.4 GHz and unlicensed 5.2 GHz bands. The excitation of dual-band resonance is explained by surface

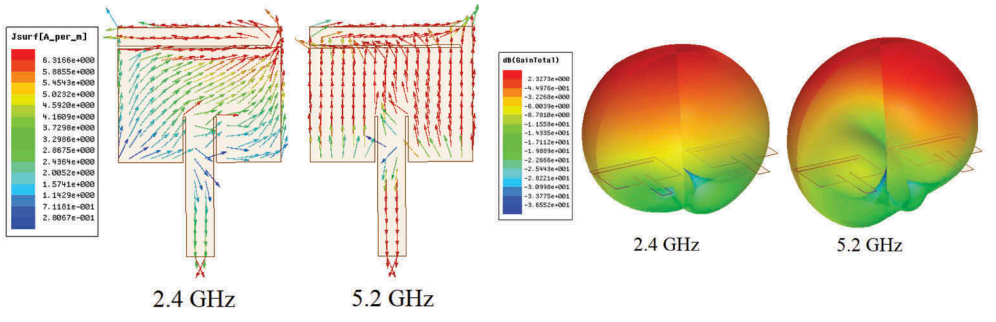

Figure 3. (a) Surface current distribution on the patch and (b) Radiations from the antenna.

current distributions on the radiator. For the ISM 2.4 GHz band, the current path is longer which crosses the rectangular slot as shown in Figure 3(a). Similarly, the shorter current path up to the slot is exciting unlicensed 5.2 GHz band. A rectangular patch antenna operating in the dominant TM_{10} mode radiates from the edges and currently follows the path along the length resulting in the perfectly broadside radiation. However, the integration of the slot is obstructing the current to flow exactly along the length, as shown in Figure 3(a). Thus, the surface current distribution is modified yielding tilted broadside radiation in both ISM bands, as depicted in Figure 3(b).

3. EBG integrated antenna

In this section, a dual-band EBG is placed between two dual-band antennas separated by a distance of $\lambda_{max}/8$, as shown in Figure 4. A mushroom type EBG structure is used as a basic structure to construct a dual-band EBG, as shown in Figure 4(c). Dual-band rejection is introduced by utilising both, top and bottom plates of a traditional mushroom type EBG. The upper metal plates are shorter which are used to create a band-gap for upper unlicensed 5.2 GHz band. Whereas, a larger single bottom plate is used to reject the lower ISM 2.4 GHz band.

However, dimensions of both plates are precisely optimised to obtain the exact frequency bands. Moreover, when the EBG structure is placed between antennas it also alters the operating frequency of the dual-band antenna. Thus, the EBG structure and antenna dimensions are synchronously optimised to obtain the desired frequency bands with improved.

The band rejection property of the dual-band EBG structure can be explained through the dispersion diagram (Figure 5(a)) and the mutual coupling (S21) (Figure 5(b)) between antennas. The relation between phase (β) and the frequency (f) is shown in Figure 5(b) which is called dispersion diagram counterpart to the Brillouin zone diagram of a crystalline periodic structure. It is evident that there are no wave propagations in the ISM 2.4 GHz and the unlicensed 5.2 GHz bands. The mutual coupling of antennas with and without EBG is shown in Figure 5(b). Both antennas are resonating at 2.4 GHz and 5.2 GHz bands resulting in strongest radiations in these two bands resulting in strong mutual coupling in the respective bands, as evident in Figure 5(b). It is noted in Figure 5(b) that even unlicensed 5.2 GHz band has smaller near-field region than ISM 2.4 GHz band,

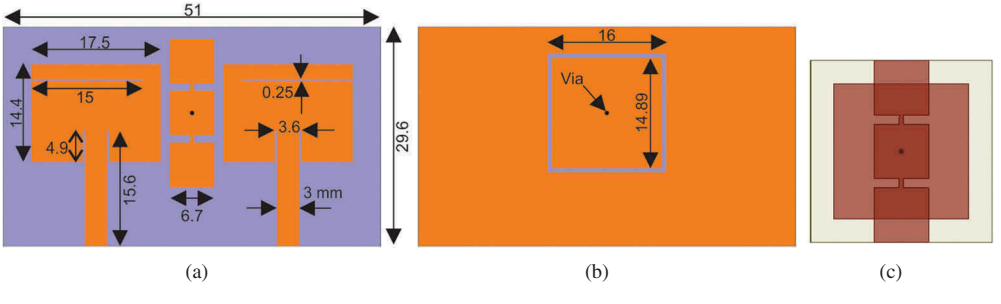

Figure 4. Layout of final design (Units mm) (a) Top view, (b) Bottom view and (c) Dual-band EBG (top view).

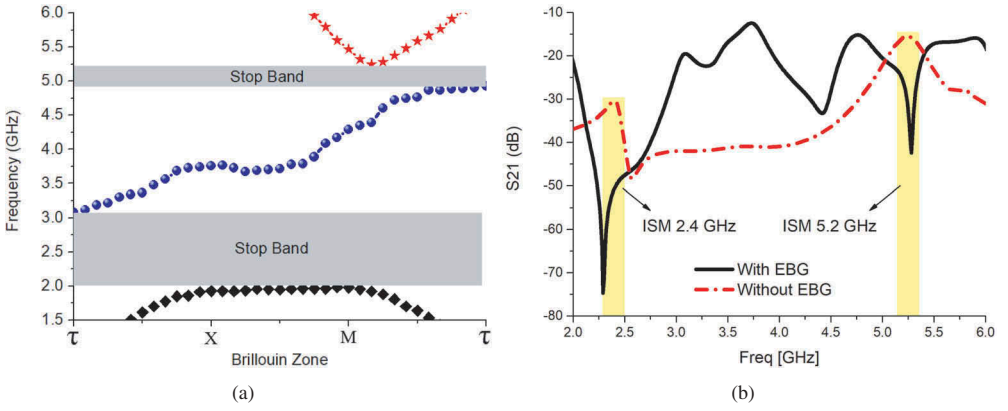

Figure 5. EBG characteristics (a) Dispersion diagram of the unit-cell and (b) Mutual coupling between dual-band antennas.

unlicensed 5.2 GHz band experience stronger mutual coupling compared to 2.4 GHz band for both with and without EBG configuration. This is due to the placement of antenna elements in mirror-image position (Figure 4(a)) resulting in current flow 180° out of phase in each element at 2.4 GHz band leading to better isolation at ISM 2.4 GHz band.

As the EBG structure is placed between antennas, the mutual coupling is sharply reduced in both operating bands which confirms the dual-band rejection characteristics of the proposed EBG structure. Moreover, as the EBG structure is placed between antennas, it slightly shifts the operating frequency in both operating bands. Hence, the dimensions of antenna elements are further optimised (Figure 4) and scattering parameters are shown in Figure 6. The other antenna parameters of the MIMO antenna with and without EBG structure are also analysed and discussed in the following sections.

4. Prototyping and experimental analysis

In this section, the prototype of the proposed antenna is fabricated and different parameters of the antenna are experimentally verified. Measured results are compared with simulated results and discussed. The simulation of the design is performed using Ansys Electromagnetic Suite. To achieve the maximum accuracy, the delta-s is set to very low (0.0001) and more number of passes (40) have been assigned in the simulator.

The scattering parameter of the antenna is measured on Agilent E8362B Vector Network Analyser and the radiation pattern of the antenna is measured using Amitec Antenna Training System in a closed chamber. The prototype of the antenna is shown in Figure 7. The fabrication of the antenna is precisely done using Computer Numerical Control (CNC) milling machine. During the prototype testing, to connect the antenna to the measuring instruments, as vector network analyser, spectrum analyser a 50 Ω Sub-miniature version-A (SMA) connector is soldered to the co-planar waveguide feeding (CPW) line of the antenna. The simulated and measured scattering parameters are shown in Figure 8. Excellent agreement can be observed between simulated and measured operating frequency bands. The prototype of the optimised structure is developed and measured results are compared with the simulated S21 (Figure 5(b), with EBG) and S11

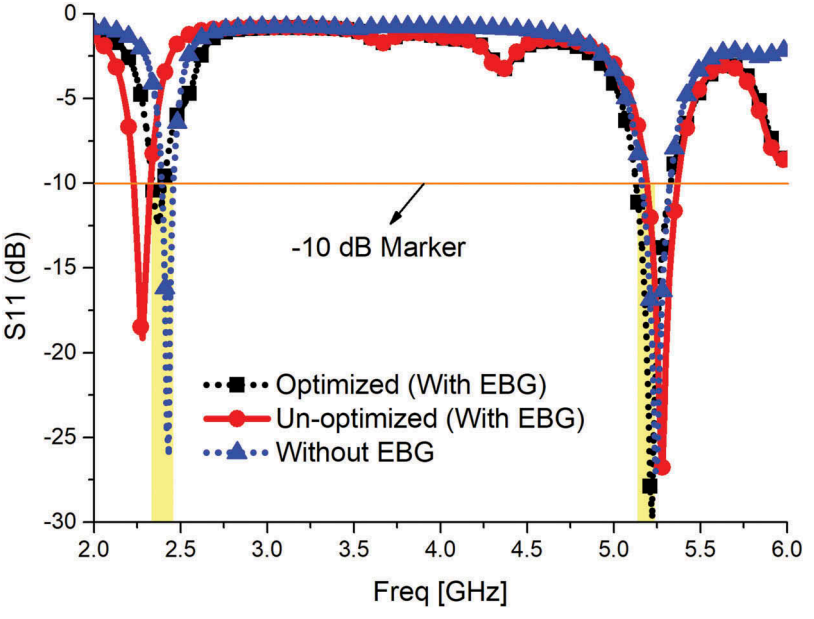

Figure 6. S11 parameter of different configuration of antennas.

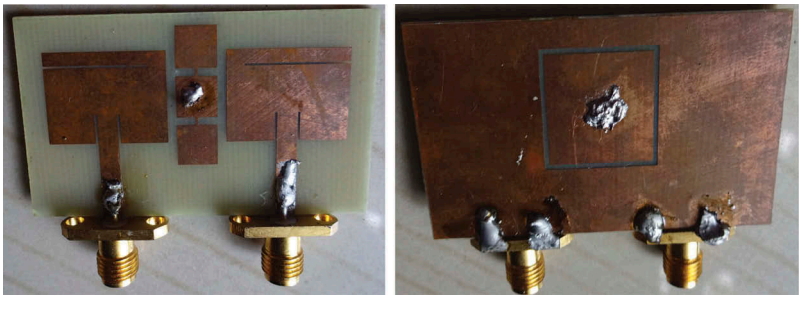

(a) (b)

Figure 7. Prototype of the final design (a) Top view and (b) Bottom view.

(Figure 6, optimised (with EBg)) in Figure 8(a,b) respectively. However, in ISM 2.4 GHz band better impedance matching is realised after fabrication. In ISM 2.4 GHz, the antenna has measured −10 dB impedance bandwidth of 70 MHz covering from 2.38 GHz to 2.45 GHz. In unlicensed 5.2 GHz, the antenna has wider −10 dB impedance bandwidth of 150 MHz covering from 5.17 GHz to 5.32 GHz. Similarly, simulated and measured mutual coupling parameters (S21) have good agreement in both ISM 2.4 and unlicensed 5.2 GHz bands hence, ensures the dual-band rejection characteristics of the proposed EBG structure. The mutual coupling of the antenna is below −60 dB and −30 dB in ISM 2.4 and unlicensed 5.2 GHz bands, respectively. Blanch et al. have presented the expressions (3) of the envelope correlation coefficient (ECC) using the input parameters S11, S12, S21, and S22 in (Blanch, Romeu, & Corbella, 2003). However, for the identical antennas, the expression (3) is simplified to (4) and other MIMO communication parameters,

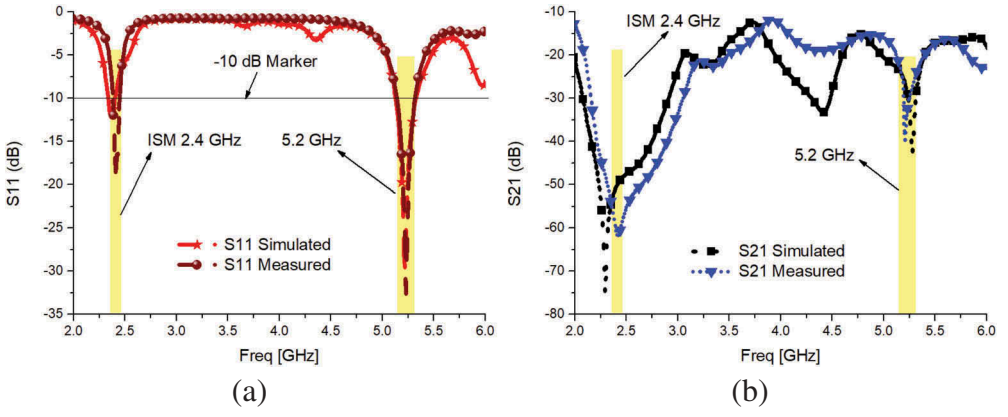

Figure 8. Simulated and measured scattering parameters (a) S11 and (b) S12.

multiplexing efficiency (η_{MUX}) (5), and diversity gain (DG) (6) are presented in (Iqbal et al., 2017):

$$ECC = \frac{|S_{11}^{*}S_{12} + S_{21}^{*}S_{22}|}{(1 - |S_{11}|^{2} - |S_{21}|^{2})(1 - |S_{22}|^{2} - |S_{12}|^{2})} \tag{3}$$

Since both antenna elements of the MIMO configuration are identical $|S_{11}| = |S_{22}|$, and $|S_{12}| = |S_{21}|$. Thus, the ECC, and η_{MUX} expressions can be rewritten as:

$$ECC = \frac{|S_{11}^{*}S_{21} + S_{21}^{*}S_{11}|}{2(1 - |S_{11}|^{2} - |S_{21}|^{2})} \tag{4}$$

$$\eta_{MUX} = \sqrt{(1 - |\rho_c|^{2})\eta^{i}} \tag{5}$$

$$DG = 10\sqrt{1 - (ECC)^{2}} \tag{6}$$

where complex correlation coefficient $(|\rho_c|) \approx \sqrt{ECC}$, η is radiation efficiency of a single element and i is a number of antenna elements. Using expressions (3–6), the MIMO communication parameters are calculated and listed in Table 1. The simulated and measured radiation pattern of the antenna is shown in Figure 9. It is evident that the proposed antenna has maximum radiation in the broadside direction for both ISM 2.4 and unlicensed 5.2 GHz bands.

The simulated and measured gain of the antenna is sown in Figure 10. The gain of the antenna is measured by two antenna technique. A couple of 2.4 GHz and 5.2 GHz antennas is used as reference antennas to measure the gain of the proposed antenna in each operating band. The proposed antenna has 2.2 dBi and 3.8 dBi measured

Table 1. Calculated MIMO communication parameters.

Frequency band	Envelope correlation coefficient (ECC)	Diversity gain (DG)	Multiplexing efficiency (η_{MUX})
2.4 GHz	0.2	9.8	0.99
5.2 GHz	0.07	9.98	0.987

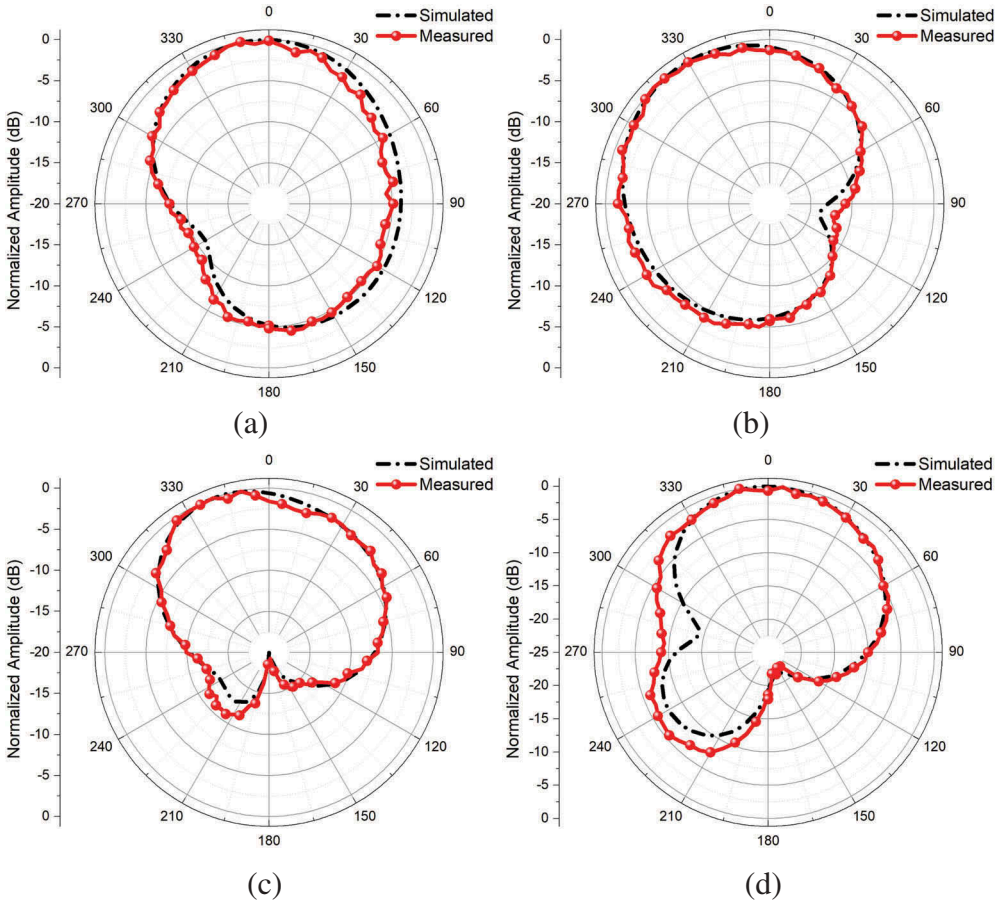

Figure 9. Radiation pattern of the antenna (a) E-plane, 2.4 GHz, (b) H-plane, 2.4 GHz, (c) E-plane, 5.2 GHz and (d) H-plane, 5.2 GHz.

realised gain in the ISM 2.4 GHz and unlicensed 5.2 GHz bands, as shown in Figure 10. The 5.2 GHz wavelength is lower than ISM 2.4 GHz but both bands are radiating from the similar structure resulting in better realised gain at higher frequency band.

5. Conclusion

A dual-band EBG integrated 1 × 2 MIMO antenna is presented. A dual-band resonance is introduced simply by incorporating an optimised rectangular slot into the radiating patch. A mushroom type EBG with two different square-shaped top and bottom plates is found effective for dual-band band rejection. The mutual coupling between closely placed two identical dual-band antenna is significantly suppressed by placing the proposed dual-band EBG. Performance of the proposed antenna is studied for MIMO communication and found satisfactory. Useful ISM 2.4 GHz, and unlicensed 5.2 GHz frequency bands are covered which makes proposed design appropriate for various wireless communication systems.

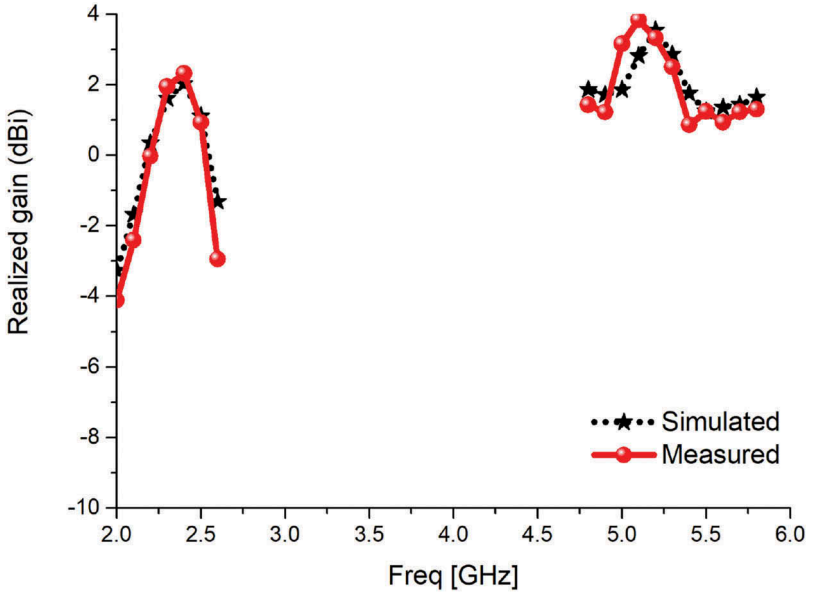

Figure 10. Simulated and measured realised gain.

Disclosure statement

No potential conflict of interest was reported by the authors.

References

Arun, H., Sarma, A. K., Kanagasabai, M., Velan, S., Raviteja, C., & Gu, M. N. (2017). Deployment of modified serpentine structure for mutual coupling reduction in MIMO antennas. *IEEE Antennas & Wireless Propagation Letter*, *13*, 277–280.

Balanis, C. A. (2012). *Antenna theory analysis and design* (3rd ed.). New York, NY: John Wiley & Sons.

Balanis, C. A. (2012). *Antenna theory analysis and design* (3rd ed.). New York, NY: John Wiley & Sons.

Bhavarthe, P. P., Rathod, S. S., & Reddy, K. T. V. (2019). A compact dual band gap electromagnetic band gap structure. *IEEE Transactions on Antennas & Propagation*, *67*, 596–600.

Blanch, S., Romeu, J., & Corbella, I. (2003). Exact representation of antenna system diversity performance from input parameter description. *Electronics Letters*, *39*, 705–707.

Caimi, F. M. (2011). Antenna design challenges for 4G. *IEEE Wireless Communication*, *18*, 4–5.

Dabas, T., Gangwar, D., Kanaujia, B. K., & Gautam, A. K. (2018). Mutual coupling reduction between elements of UWB MIMO antenna using small size uniplanar EBG exhibiting multiple stop bands. *International Journal of Electronics and Communications (Aeäœ)*, *93*, 32–38.

Gholipour, M., Azadi-Tinat, N., & Ghalibafan, J. (2019). Simple EBG surface for X-band radar cross section reduction. *International Journal of Electronics & Communications (Aeäœ)*, *100*, 47–55.

Hwangbo, S., Yang, H. Y., & Yoon, Y. (2017). Mutual coupling reduction using micromachined complementary meander line slots for a patch array antenna. *IEEE Antennas & Wireless Propagation Letter*, *16*, 1667–1670.

Iqbal, A., Saraereh, O. A., Ahmad, A. W., & Bashir, S. (2017). Mutual coupling reduction using F-shaped stubs in UWB-MIMO antenna. *IEEE Access*, *6*, 2755–2759.

Jaglan, N., Gupta, S. D., Thakur, E., Kumar, D., Kanaujia, K. B., & Srivastava, S. (2018). Triple band notched mushroom and uniplanar EBG structures based UWB MIMO/Diversity antenna with

enhanced wide band isolation. *International Journal of Electronics & Communications (Aeãœ)*, *90*, 36–44.

Jiao, T., Jiang, T., & Li, Y. (2017). Antenna array coupling reduction based on stacked EBG structures. *International Applied Computational Electromagnetics Society Symposium (ACES)*, *Suzhou, China*.

Kumar, J. (2016). Compact MIMO antenna. *Microwave Optical Technology Letter*, *58*, 1294–1298.

Kumar, J., & Shirgan, S., S, (2014). Compact partial ground plane 1 × 2 patch antennas. *Sixth International Conference on Computational Intelligence and Communication Networks*, Bhopal, India. (pp. 33–37).

Li, J., Zhang, X., Wang, Z., Chen, X., Chen, J., Li, Y., & Zhang, A. (2018). Dual-band eight-antenna array design for MIMO applications in 5G mobile terminals. *IEEE Access*. doi:10.1109/ACCESS.2019.2908969

Luo, S., Li, Y., Xia, Y., Yang, G., Sun, L., & Zhao, L. (2019). Mutual coupling reduction of a dual-band antenna array using dual-frequency metamaterial structure. *Applied Computational Electromagnetics Society Journal*, *34*, 403–410.

Luo, S., Li, Y., Xia, Y., & Zhang, L. (2018). A low mutual coupling antenna array with gain enhancement using metamaterial loading and neutralization line structure. *Applied Computational Electromagnetics Society Journal*, *34*, 411–418.

Mohamadzade, B., & Afsahi, M. (2017). Mutual coupling reduction and gain enhancement in patch array antenna using a planar compact electromagnetic bandgap structure. *IET Microwave, Antennas & Propagation*, *11*, 1719–1725.

Park, C. H., Son, H. W., & Raj, K. S. (2017). Mutual coupling reduction between closely spaced microstrip antennas by means of H-shaped conducting wall. *Electronics Letter*, *13*, 1093–1094.

Vishvaksenan, K. S., Mithra, K., Kalaiarasan, R., & Raj, K. S. (2017). Mutual coupling reduction in microstrip patch antenna arrays using parallel coupled-Line resonators. *IEEE Antennas & Wireless Propagation Letter*, *16*, 2146–2149.

Xia, Y., Chen, X., & Tang, T. (2015). A novel eight ports dual band antenna array for 2.4/3.5 GHz MIMO applications. *Optik*, *126*, 1175–1180.

Yang, F., & Samii, Y. R. (2003). Microstrip antennas integrated with electromagnetic band-gap (EBG) structures: A low mutual coupling design for array applications. *IEEE Transactions on Antennas & Propagation*, *51*, 2936–2946.

Yu, K., Li, Y., & Liu, X. (2018). Mutual coupling reduction of a MIMO antenna array using 3-D novel meta-material structures. *Applied Computational Electromagnetics Society Journal*, *33*, 758–763.

Zhao, L., Liu, F., Shen, X., Jing, G., Cai, Y., & Li, Y. (2017). A high-pass antenna interference cancellation chip for mutual coupling reduction of antennas in contiguous frequency bands. *IEEE Access*. doi:10.1109/ACCESS.2018.2853709

Zhu, J., & Eleftheriades, G. (2010). A simple approach for reducing mutual coupling in two closely spaced metamaterial-inspired monopole antennas. *IEEE Antennas & Wireless Propagation Letter*, *9*, 379–382.